JTTEE5 14:502-510
DOI: 10.1361/105996305X76522
1059-9630/$19.00 © ASM International

Particle Size Distribution in a Wire-Arc Spraying System

A. Pourmousa, J. Mostaghimi, A. Abedini, and S. Chandra

(Submitted October 26, 2004; in revised form March 12, 2005)

The size and velocity of particles produced by a ValuArc 200 (Sulzer-Metco, Westbury, NY) twin-wire-arc spraying system were measured in-flight using a DPV-2000 system (Tecnar Ltd., St-Bruno, QC, Canada) for a range of operating parameters. A technique was developed to identify and separate the size distributions of particles produced by atomization of molten metal at either the anode or the cathode by assuming that both follow a log-normal distribution. It was shown that particles produced by the anode are almost two times larger in diameter than those originating from the cathode. Experiments showed that increasing the pressure of atomizing gas decreased the size of both anodic and cathodic particles, but changing wire feed rate and operating voltage did not change particle size significantly.

Keywords diagnostics and control, size distribution, twin wire-arc spray

1. Introduction

Twin wire-arc spraying is an economical spraying process that has become popular in the thermal spray industry because it combines low operating and equipment costs with high deposition efficiencies. Wire-arc coatings, though, are usually of poorer quality than those obtained from other methods such as plasma spraying and high-velocity oxyfuel spraying (HVOF), with greater porosity and lower adhesion strength. A better understanding of the spray process will provide us with some guidelines as to how existing wire-arc spray equipment designs can be modified to improve coating properties.

The quality of thermal sprayed coatings is directly related to the properties of the molten particles such as size, temperature, and velocity (Ref 1-4). These are not independent since the diameter of particles determines the magnitude of both heat transfer and drag forces acting on them and thus their temperature and velocity. In powder-based spray techniques such as plasma spraying or HVOF, particle size is determined by the size distribution of the powder fed into the gun. Wire-arc spraying is different because no powder is used; rather, the heating of the wire tips by the arc and detachment of molten metal droplets caused by drag and magnetic forces determines the shape and size of spray particles. It has long been known that anode and cathode are heated differently in a wire-arc process. The arc attaches to the anode over an area larger than the cathode where heating is more localized at the cathode spot (Ref 4, 5). At the tip of the anode wire, a large area is heated due to diffuse arc-anode attachment, melting a layer of metal that is pushed off the edge of the wire-tip by the atomizing gas, creating an "anode sheet." At the cathode, constricted arc attachment causes much more localized heating and melting. Also, because the current passes through a smaller area, the current density (j) at the cathode surface is much higher, producing a large magnetic pinch force (or $j \times B$ force where B is the induced magnetic field). Molten metal droplets ejected into the arc from the cathode by both drag and magnetic forces are observed to be smaller than those detaching from the anode. Using laser strobe photography, Hussary et al. (Ref 5, 6) and Watanabe et al. (Ref 7, 8) clearly illustrated the differences between molten metal detachment at the tips of the anode and cathode wires. Inhomogeneity in the microstructure of wire-arc coatings was also observed by Zhu et al. (Ref 9). It was demonstrated that particles originating from anode and cathode are distributed in an asymmetric way about the centerline of the wire-arc spray.

In the most complete attempt, to date, to model particle production in the wire-arc spraying process (including atomizing gas in the nozzle, an electric arc in the presence of crossflow, and primary and secondary atomization), Kelkar et al. (Ref 10, 11) used the traditional particle breakup model of Amson (Ref 12) and Arai and Hashimoto (Ref 13). More recently, Hussary et al. (Ref 6) studied the mechanisms involved in primary atomization of molten metal from the wire tips and the effect of varying process parameters on these mechanisms. This study presented quantitative predictions about sheet, extrusion and membrane lengths, and breakup times.

Several different researchers have noted the bimodal size distribution of wire-arc spray particles (Ref 6, 10, 11). However, no quantitative analysis has been done to measure the variation of particle size. The aim of this study was to measure the size distribution of wire-arc particles and confirm the dual peak size distribution of particles, to develop a technique to separate the individual peaks in the bimodal size distribution, and to investigate the effect of process parameters on the size distribution of particles originating from each electrode.

2. Experimental Apparatus

The results presented in this paper were obtained using ValuArc 200 twin-wire-arc spraying system with high-velocity air cap, manufactured by Sulzer-Metco Inc. (Westbury, NY). The

A. Pourmousa, J. Mostaghimi, A. Abedini, and **S. Chandra,** Centre for Advanced Coating Technologies (CACT), University of Toronto, 5 King's College Road Toronto, Ontario, M5S 3G8, Canada. Contact e-mail: purmusaa@mie.utoronto.ca.

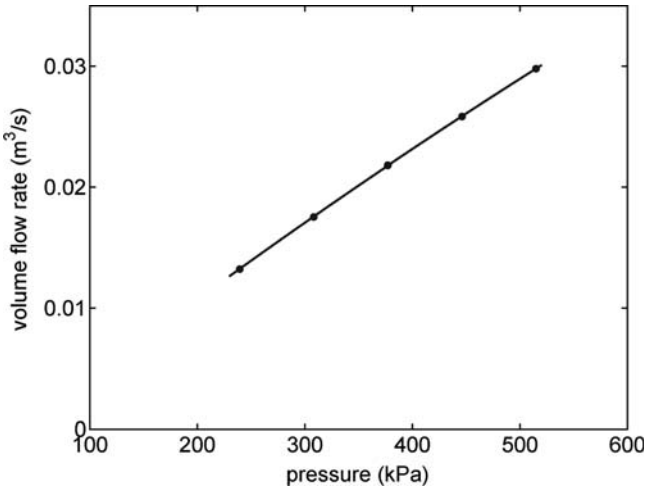

Fig. 1 Volume flow rate of the atomizing gas (dry air) as a function of pressure

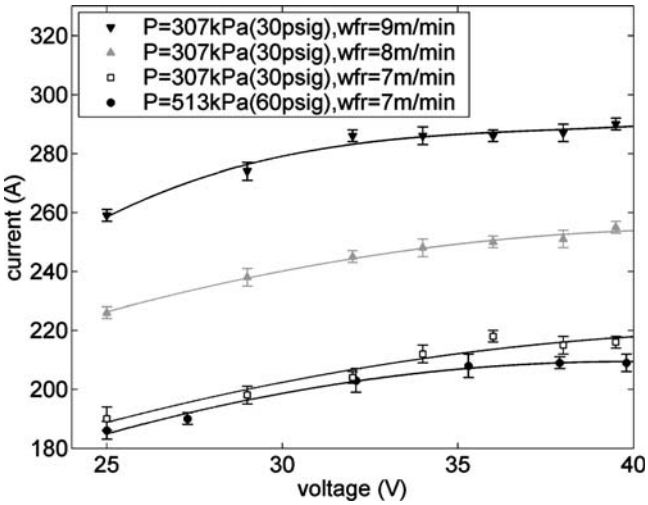

Fig. 2 Current-voltage characteristic of the arc for different wire-feed-rates (termed as *wfr*) and pressures; the error-bars represent current fluctuation and standard deviation of 5-10 measurements.

operating parameters of this system and their working ranges are listed below:

- Voltage can be varied from 20 to 40V.
- Wire-feed-rate can be varied from 3 to 10 m/min (0.05 to 0.17 m/s).
- The following 14-gauge wires (d = 1.6 mm), manufactured by Sulzer-Metco, were used:
  (a) Stainless Steel Metcoloy 2: Fe 13Cr 0.5Si 0.5Ni 0.5 Mn 0.35C
  (b) Stainless Steel Metcoloy 5: Fe 18Cr 8.5Mn 5Ni 1Si 0.15C
  (c) Metco Al: 99% aluminum
  (d) Metco Copper AW: 99.8% copper
- Pressure of the atomizing gas can be varied from 239 to 550 kPa (20 to 65 psig). The volume flow rate of the gas increases linearly with pressure (Fig. 1).
- The atomizing gas is dry air.

The system uses an LCARE electric-arc power supply (Sulzer-Metco) with a controllable output direct current (dc) voltage. The current that passes through the arc is determined by the operating parameters (Fig. 2). An external flow-meter and pressure gage (MEM Thru View, Meter Equipment Manufacturing, Willoughby, OH) was installed upstream of the gas-inlet hose of the spraying gun to measure the volume flow rate and pressure of the atomizing gas. The pressure gauge was installed between the flow meter and the spraying gun.

The DPV-2000 monitoring system (Tecnar Ltd., St-Bruno, QC, Canada), was used to measure in-flight particle velocity, temperature, and size distributions. The DPV-2000 is an optical instrument that determines the properties of individual particles by measuring the infrared radiation emitted by each particle passing through the field-of-view of its sensing head. A mask with two slits is fixed in front of the optical sensor so that two peaks are recorded whenever a particle is detected. Particle velocity is measured by recording the time taken for each particle to traverse the known distance between two slits; diameter by measuring the total radiation emitted by each particle and assuming it is a spherical gray body emitter; and temperature by using principles of two color pyrometry (Ref 14).

DPV particle size measurements were calibrated by spraying wire-arc particles into water, drying them, and washing with acetone. Figure 3 shows a typical sample of such particles. The size distribution of the powder collected was measured using a particle size analyzer (MasterSizer S; Malvern Instruments Ltd., Malvern, UK) with a detection range from 0.05 μ to 880 μm, and then fitted to the DPV-2000 size distribution by varying the assumed diameter coefficient of the DPV software, a factor that takes the effect of material emissivity into account (Ref 14). Particle size distributions were plotted as both frequency-histogram and volumetric-histogram of particle diameter, assuming particles were spherical.

3. Spatial Characteristics of the Spray

The wire-arc spraying system with a high-velocity air cap has a divergence angle of about 15°, giving a coated area of 50 × 50 mm when the substrate is placed 200 mm away from the gun. The deposited coating is not a perfect circle; rather, the spray pattern is in the shape of an oval whose shorter radius lies in the plane of the two wires. For example, the minor and major radii of the coated area are 25 and 30 mm, respectively, for a substrate at a stand-off distance of 200 mm (with V = 32.1 V, p = 308 kPa, and wire feed rate = 7 m/min). This is because the atomizing gas stream is diverted by the wires producing a spray divergence that is larger along the x-axis than it is along the y-axis (Fig. 4a).

Particle properties were measured at different positions in the spray to examine the uniformity of the spray. Figure 4 shows the variation of particle velocity (Fig. 4a) and diameter (Fig. 4b) at different x and y positions in the spray at a distance of 50 mm from the spray nozzle. Results are shown for aluminum particles with the operating parameters of the gun kept constant with a gas pressure of 308 kPa, arc voltage of 32.1 V, and wire feed rate of 7 m/min. The points in Fig. 4 represent the average of 3-5 measurements of 7000-10,000 particles in the spray, and the error bars show the standard deviation of the values recorded.

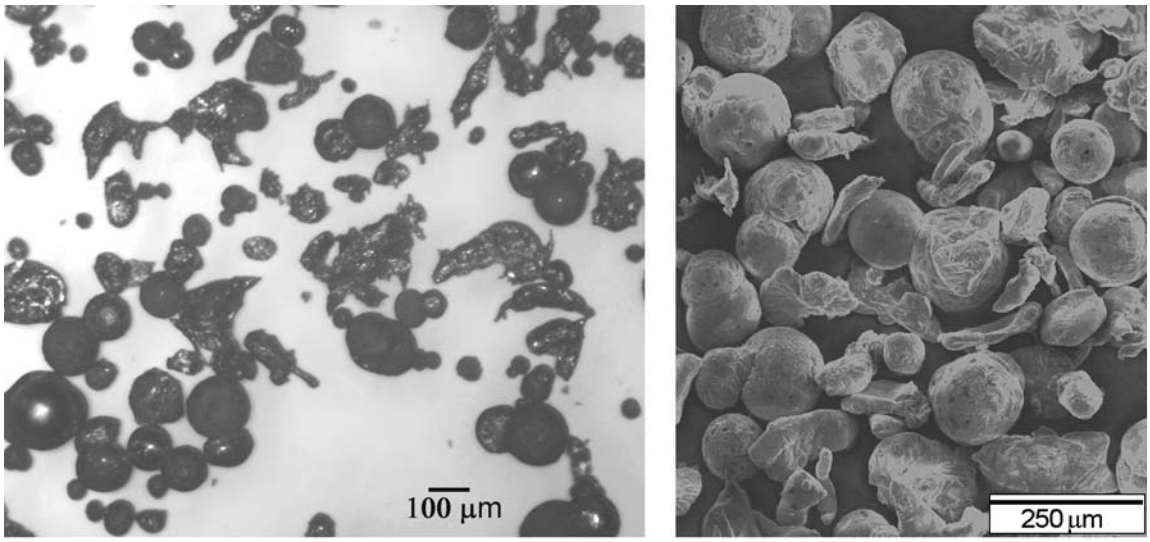

Fig. 3 (a) Optical and (b) SEM pictures of aluminum particles collected by spraying into water; p = 308 kPa, V = 32.1 V, wire feed rate = 7 m/min

Particle velocity diminished with distance from the centerline of the spray (Fig. 4a), following the gas velocity profile (Ref 15). The average particle diameter increased with increasing radial distance from the centerline of the spray (Fig. 4b) because the off-center particles experienced less of the secondary-atomizations in the low-velocity gas flow. Particle temperatures (not plotted here) were practically constant in the x-y plane (about 2433 K), and any variations were within the experimental error range. Particle temperature was much higher than the melting point of aluminum, indicating that surface oxidation produced a highly exothermic reaction on the surface of particles.

Mass flow-rate of particles ($\dot{m}$) at any axial location in the plume can be calculated:

$$\dot{m} = \dot{n} \cdot \rho \cdot \frac{\text{Average}\left(\frac{v \cdot \pi d^3}{6}\right)}{\text{Average}(v)} \qquad \text{(Eq 1)}$$

where d and v are diameter and speed of a particle, ρ is the density of the particles, and $\dot{n}$ is the number flow-rate (number of particles per second that pass through the field of view of the DPV-2000 sensing head). Because the DPV-2000 system records only a certain fraction of particles (depending on the settings and detection criteria) passing through its sensing volume, the number flow-rate of particles measured is proportional to the actual value. Therefore, the calculated mass flow-rate will be a relative (or scaled) value. Figure 4(c) illustrates the relative mass-flow-rate profile of the in-flight particles at a cross-section of the spray.

A measure of the spatial dispersion of particles is the full width at half-maximum (FWHM) of the mass flow-rate curve, defined as the distance between points on the mass-flow rate curve at half the peak value. The FWHM of particle mass flow rate in the y direction is about 28 and 35 mm in the x-direction (Fig. 4c), producing the elliptical deposit on the substrate observed in experiments.

When the DPV-2000 was calibrated, the size of particles sprayed into water was matched to those measured by the DPV along the axis of the spray. Radial variations of particle size, such as those shown in Fig. 4(a), were ignored in this process. Neglecting particle size variations does not create a large error because the particle density in the spray is concentrated along the spray axis (Fig. 4c). It was estimated that the error in total mass flow rate introduced by assuming uniform particle size distribution was less than 4%.

Variation of particle properties along the axis of the spray gun was also investigated. Velocity of particles decreased with distance form the nozzle, falling from 160 m/s at z = 70 mm to about 100 m/s at z = 200 mm. Particle size distribution and temperature showed no variation in the z direction. It is speculated that heating of aluminum particles caused by surface oxidation offsets the cooling caused by convection and radiation to the surroundings.

4. Particle Size Distribution

In the wire-arc spraying system, the arc attaches differently to the anode and cathode (Ref 4, 5, 7, 8, 10, 11, 16, 17), so the two wires do not melt in the same way. Photographs of arcs have shown that cathode heating is confined to a small area (cathode spot), but the anode is heated more uniformly, though in both cases the area of arc attachment is smaller than the diameter of the wire (Ref 5-7). Droplets detaching from the anode are therefore typically larger than those from the cathode (Ref 5, 8), producing a dual-peak particle size distribution. In some recent studies (Ref 6, 10), bimodal size-distribution have been reported when operating with low atomizing gas pressures. However, at higher pressures, the two peaks overlap so it is not easy to distinguish between them. Figure 5(a) shows the diameter frequency-histogram of aluminum particles produced with atomizing gas pressure 515 kPa, arc voltage 37.9 V, and wire feed rate = 7 m/min. The same data is presented as a volumetric-

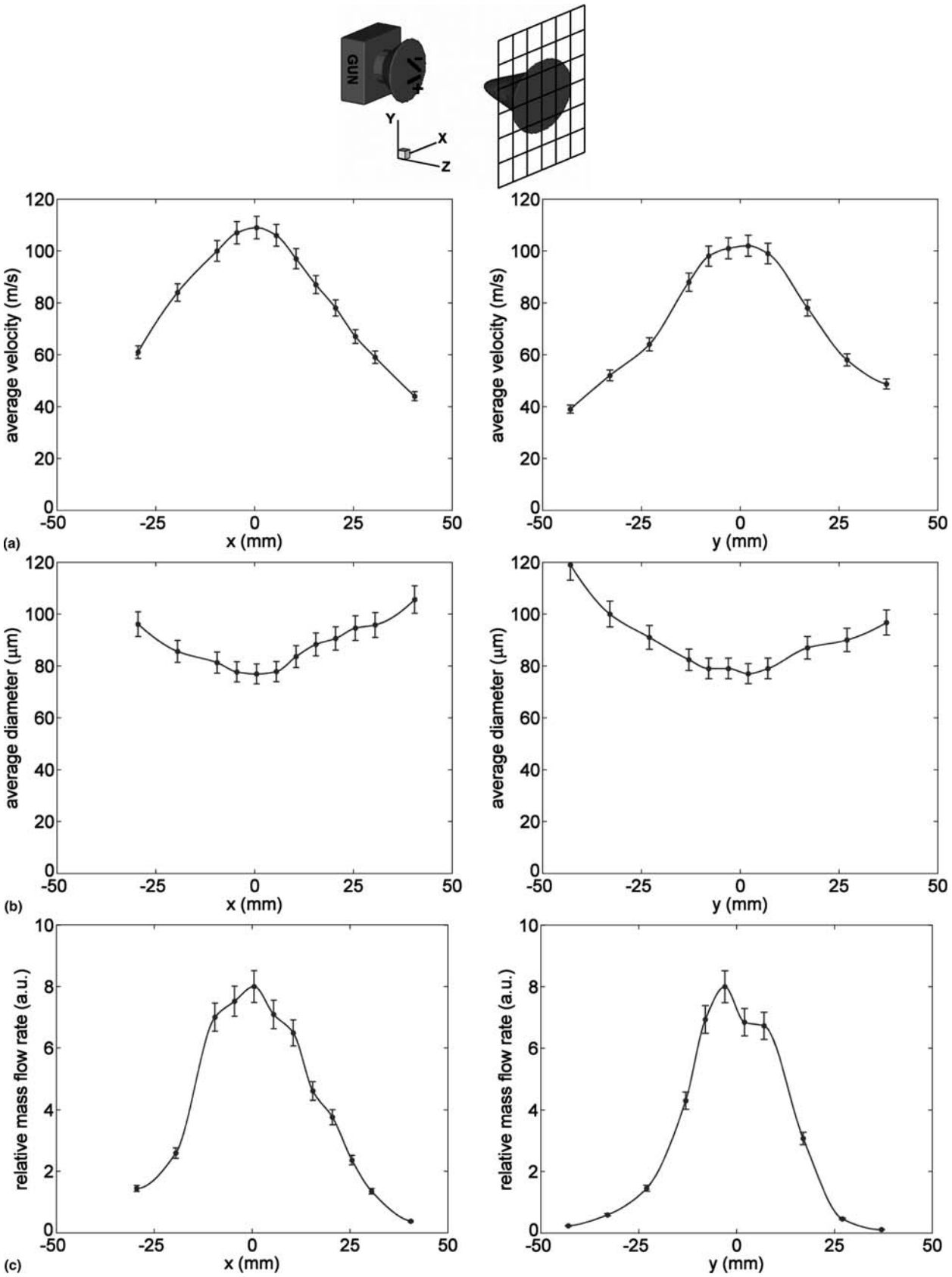

Fig. 4 (a) Velocity, (b) diameter, and (c) mass-flow-rate of the spray particles as a function of y and x, with $z = 50$ mm; center of the spray is located at $x = y = 0$ mm; the error-bars in the graphs represent the standard deviation of 3-5 measurements.

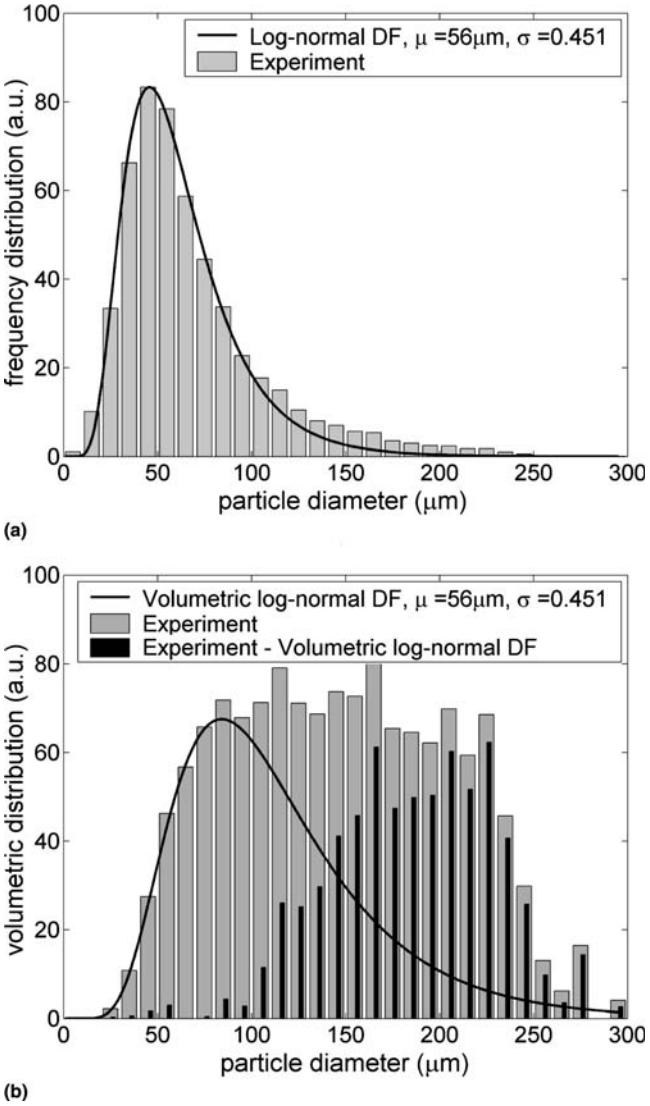

Fig. 5 (a) Frequency-distribution and (b) volumetric-distribution histograms of measured particle diameter are shown by grey histograms; p = 515 kPa, V = 37.9 V, and wire-feed-rate = 7 m/min. The curve in (a) is a log-normal function (μ = 56 mm, σ = 0.451) matching the maximum and full-width-half-maximum of the measured distribution. The curve in (b) is the volumetric log-normal function with the same μ and σ as (a) and scaled with the same scaling factor as the measured volumetric-distribution. The black bar-histogram represents the difference between the measure volumetric-distribution and the volumetric log-normal function.

histogram (volume fraction) in Fig. 5(b). The y axes in the size distributions are shown with arbitrary units because only a fraction of all particles in the spray were recorded by the DPV-2000. Only one peak is obvious in both cases. The technique used to separate cathodic and anodic particles is described below.

4.1 Size Distribution of Anodic and Cathodic Particles

The size distribution of particles produced by atomization of liquid jets typically follows a log-normal probability distribution function defined by (Ref 18):

$$f(D) = \frac{dN}{dD} = \frac{1}{\sqrt{2\pi}\sigma}\frac{1}{D}e^{-\frac{1}{2}\left(\frac{\ln(D)-\ln(\mu)}{\sigma}\right)^2} \quad \text{(Eq 2)}$$

where s and m are the geometric standard deviation and geometric mean drop size (Ref 18, 19). This curve fits best to the experimental data of Fig. 5(a) with m = 56 mm and s = 0.451. However, there are more large particles than expected in the experiments (Fig. 5a, d > 100 mm). The difference becomes more obvious when the volumetric log-normal probability distribution function defined as:

$$vdf(D) = \frac{dV}{dD} = \frac{\pi D^3}{6}f(D) = \frac{1}{\sqrt{72\pi^{-1}}\sigma}D^2 e^{-\frac{1}{2}\left(\frac{\ln(D)-\ln(\mu)}{\sigma}\right)^2} \quad \text{(Eq 3)}$$

is plotted on the experimental volumetric-distribution data in Fig. 5(b). In this figure, the volumetric log-normal function is produced with the same m and s as in Fig. 5(a) and is scaled the same as the experimental data. Here, the difference between the number of large particles measured and those expected from typical atomization theory becomes obvious. The difference (black bar-histograms in Fig. 5b) is evidence of two sets of particles, produced by the cathode and anode, respectively, which have different but overlapping size distributions. Because particles in each of the two sets are produced by a simple atomization process in one electrode, their size distributions are expected to follow a log-normal function.

To confirm that particles produced by melting and atomization of each of the wire tips follow a log-normal probability distribution function, it was necessary to physically separate the anodic and cathodic particles. For this purpose, Stainless Steel Metcoloy 2 and Metco Copper wires were used as the anode and cathode, respectively. After being sprayed into water, particles were collected, dried, washed with acetone, and then separated using a magnet. Stainless steel and copper are distinguishable by their color under a microscope, and inspection showed that the number of copper particles present in the stainless steel particles after separation was less than 1%. To avoid particle agglomeration, stainless steel particles were placed in a demagnetizer (DEMAG, Nortronics).

Size distributions of both copper and stainless steel particles were measured using a Particle Size Analyzer (Master Sizer S; Malvern Instruments Ltd., Malvern, UK). Figure 6 shows the size distribution of anodic stainless steel particles. A log-normal distribution curve fit the data well; discrepancies were less than the uncertainty of the measuring instrument (error bars in Fig. 6). The experiment was repeated with the polarity of wires switched to that the cathode was stainless steel. Cathodic particles also follow a log-normal distribution function.

4.2 Separation Technique

The size-distribution of wire-arc particles can be represented by superposing two log-normal distribution functions. Because anode and cathode wires are fed into the spray gun at the same rate in experiments, the total masses of cathodic and anodic particles in any sample collection are equal. Therefore, even though the volumetric-distribution curves of anodic and cathodic particles are different, the area under the curves must be the same.

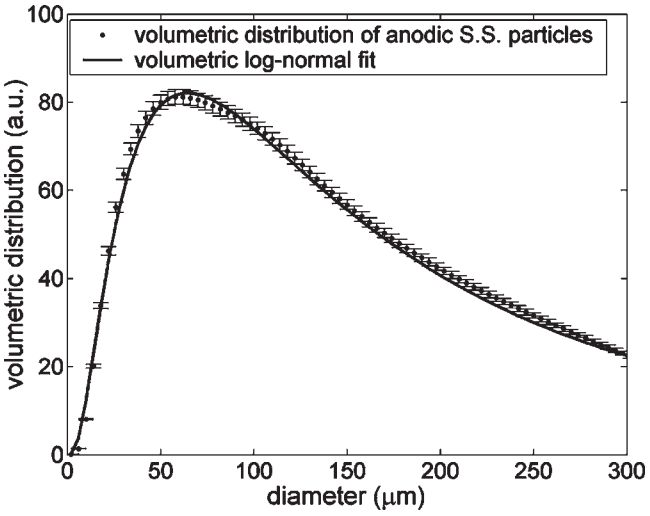

Fig. 6 The log-normal function fits well within the error-bars of the size-distribution of anodic particles. Stainless steel and copper wires were used as anode and cathode, respectively. The error bars represent the systematic-error of the size measuring device.

Because cathodic particles are smaller, they must be more numerous than the larger anodic particles. A method for determination of the size distributions of anodic and cathodic particles produced by a wire arc spray is summarized in the following steps:

1. Plot the experimental volumetric-distribution of particles and determine the area (A_0) under the curve.
2. Fit a log-normal function, using the least square method, to the ascending portion of the experimental frequency-distribution curve of particle diameter (from 0 to the most frequent particle diameter; e.g., from 0 to 45 mm in Fig. 5a). Because this fit represents the frequency-distribution of cathodic particles, the area under its volumetric-distribution curve must equal $A_0/2$. We assume here that the anodic particles are larger and much fewer in number and hence contribute little to the population of small particles.
3. Subtract the fitted cathodic distribution curve from the measured distribution to obtain the distribution of anodic particles.
4. Fit a log-normal function through the calculated diameter frequency-distribution of anodic particles using the least-squares method. The area under its volumetric-distribution curve must also be $A_0/2$.
5. Add the cathodic and anodic distributions and compare with the experimental size distribution to evaluate errors.

4.3 Error Estimation

To estimate the errors associated with the experimental instrumentation for measuring powder size distributions, two powders of known size distribution were mixed, the size distribution of the mixture was measured, and then the size distribution of one of the original powders was calculated. Metco 54NS-1 powder (Al 99%, particle size: −75 + 45 μm) was sieved to isolated batches with diameter ranges of −53 + 45 μm and −75 + 63 μm. A particle size analyzer (MasterSizer S, Malvern Instruments Ltd., Malvern, UK) was used to measure the size distributions of both samples. Equal weights of both powders were then mixed, and the size distribution of the mixture determined. Because the volume of the mixture was twice the volume of the samples, their size distributions were scaled similar to steps 1 and 2 of the algorithm outlined above. By subtracting the size distribution of the smaller particle sample from that of the mixture, the size distribution of the larger powder was determined. The relative error (ε) was calculated:

$$\varepsilon = \frac{\int |y - y_{\text{reconst}}| dx}{\int |y| dx} \quad \text{(Eq 4)}$$

where y and y_{reconst} are the experimental and calculated size distribution of the larger diameter powder, respectively. The relative error in reconstructing the size distribution was less than 4%.

To estimate the errors associated with the proposed technique for separating anodic and cathodic particle size distributions, two peaks were reconstructed from the mathematical sum of two known log-normal functions. Typical values of $\mu_1 = 50$ μm and $\sigma_1 = 0.45$ were assumed for the cathodic log-normal particle size distribution function and $\mu_2 = 120$ μm and $\sigma_2 = 0.45$ for the anodic distribution function. These curves and their summations are shown in Fig. 7, both as frequency-distribution (Fig. 7a) and volumetric-distribution (Fig. 7b) of particle diameter. Following the procedure outlined above the anodic and cathodic particle diameter distributions were reconstructed from the combined curve; the calculated size distributions are also shown in Fig. 7. The relative errors of both reconstructed functions were calculated to be less than 0.5%. This error varies with the shape and peak to peak spacing of the anodic and cathodic distribution curves. Table 1 lists five different anodic log-normal functions and the error in reconstructing them while the cathodic particle size distribution was held constant. Errors increase when the peaks are closer together and there is greater overlap of the two distribution curves.

5. Effect of Varying Wire-Arc Parameters

To investigate the effect of wire-arc operating parameters such as atomizing gas pressure, wire feed rate, and operating voltage on particle size distribution, a series of experiments was done in which each of these was varied. Particle size distributions were measured using the DPV 2000 and anodic and cathodic particles identified using the separation technique described above. Figure 8 shows a typical result for a spray gun operated with gas pressure 515 kPa, wire feed rate 7 m/min, and arc voltage 32.1 V. Particle sizes are shown as both a frequency-distribution (Fig. 8a) and volumetric-distribution (Fig. 8b), and calculated anodic and cathodic particle size distributions are also shown. Similar experiments were performed for atomizing gas pressures ranging from 239 to 515 kPa, wire feed rates of 6 to 10 m/min, and arc voltages of 25 to 40 V. Repeated experiments were performed at each setting. The results shown are the aver-

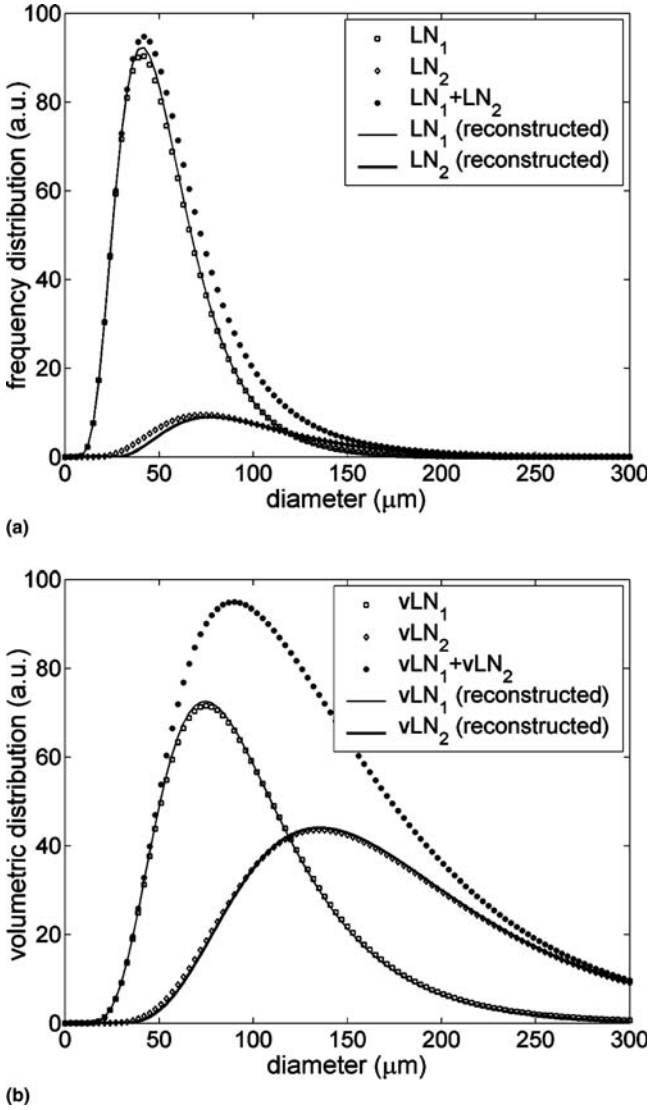

Fig. 7 The separation technique was applied on the addition of two known log-normal functions (LN_1: $\mu_1 = 50$ μm, $\sigma = 0.45$ and LN_2: $\mu_2 = 90$ μm, $\sigma = 0.45$) to reconstruct the original functions: (a) frequency-distribution and (b) volumetric-distribution.

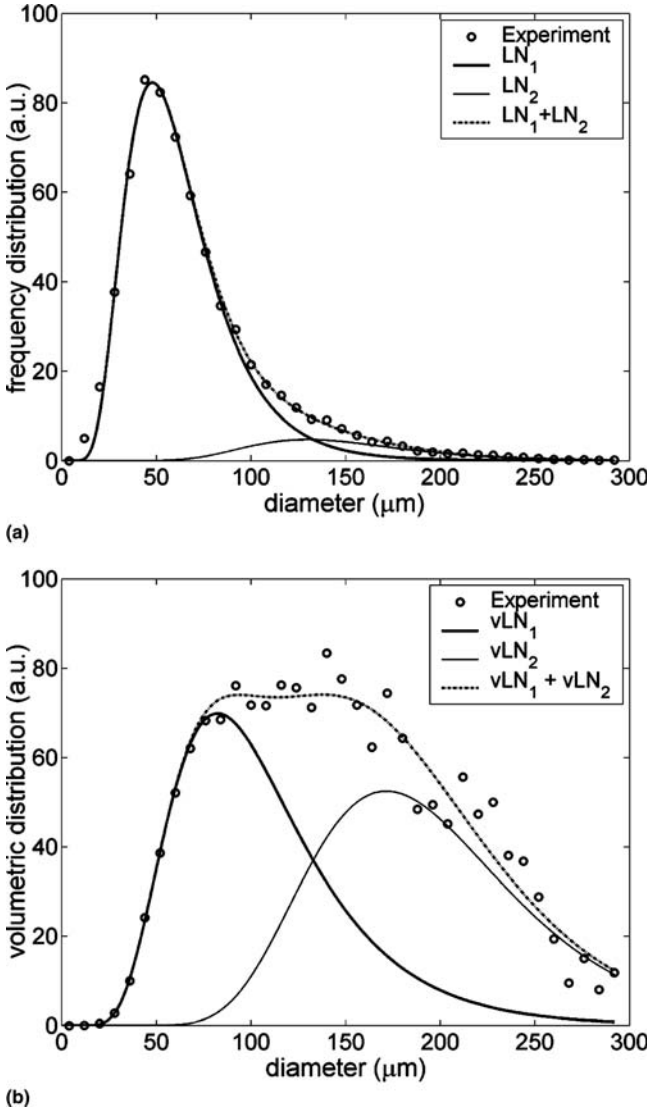

Fig. 8 Two peaks in the measured diameter distribution were separated and presented in (a) frequency and (b) volumetric forms. LN_1 and LN_2 represent log-normal distribution functions of cathodic and anodic particles, respectively. vLN_1 and vLN_2 are the volumetric representation of LN_1 and LN_2. Experimental particle size statistics were obtained by a DPV-2000 system at a stand-off distance of 50 mm, voltage of 32.1 V, wire-feed-rate = 7 m/min, and $p = 515$ kPa. These distributions represent statistics of about 8000 aluminum particles.

Table 1 Different log-normal functions and the relative error in reconstructing them from their sum

Cathodic log-normal function		Anodic log-normal function		Relative error, %
μ_1, μm	σ_1	μ_2, μm	σ_2	
50	0.45	150	0.45	0.2
50	0.45	120	0.45	0.4
50	0.45	90	0.45	1.6
50	0.45	80	0.45	3
50	0.45	70	0.45	8

age of four measurements and error bars represent the standard deviation.

Figure 9 shows the variation of both mean-diameter and mass-mean-diameter of both anodic and cathodic particles with gas pressure. Mass-mean-diameter is defined as $MMD = (\sum m_i d_i)/\sum m_i$, where m_i and d_i are mass and diameter of the ith-particle, and the summation is over all particles (Ref 6). Anode particles were always significantly larger than cathodic particles. Particle size increased as gas pressure was reduced. Drag forces exerted by the gas are the main reason for atomization of molten material from the wire tips. Droplets of molten metal are formed when drag and magnetic forces tearing liquid off the wire tip exceed surface tension forces attaching it to the wire. As gas pressure decreases, so does its velocity and therefore drag forces. Molten metal droplets grow larger before detaching from the wire tip when drag forces diminish. Moreover, secondary atomizations that break the molten material into smaller droplets

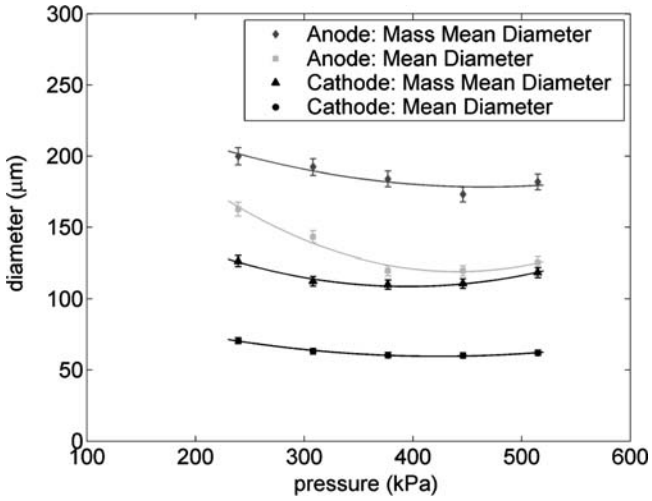

Fig. 9 Mean-diameter and mass-mean-diameter of cathodic and anodic particles decrease as the pressure of the atomizing gas increases. Anodic particles are more significantly affected by atomizing gas pressure than the cathodic particles. Error-bars represent a standard deviation of 3-5 measurements of about 8000 particles; operating parameters: aluminum wires, V = 32.1 V, wire-feed-rate = 7 m/min, stand-off distance = 50 mm.

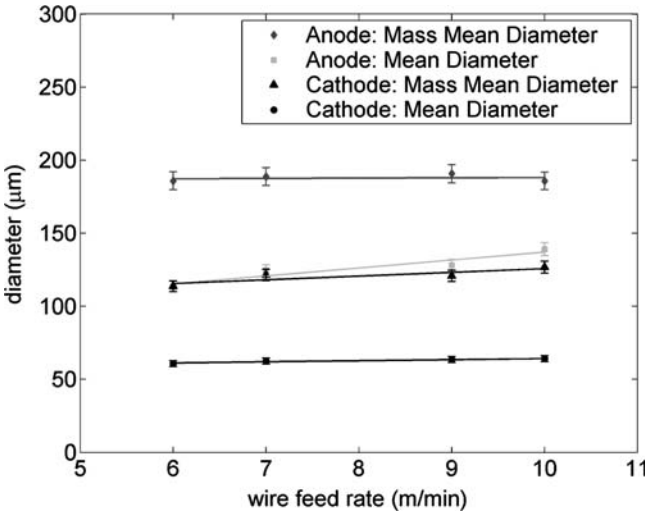

Fig. 10 Mean-diameter and mass-mean-diameter of cathodic and anodic particles as a function of the wire-feed-rate; error-bars represent a standard deviation of 3-5 measurements of about 8000 particles; operating parameters: aluminum wires, p = 515 kPa, V = 32.1 V, stand-off distance = 50 mm.

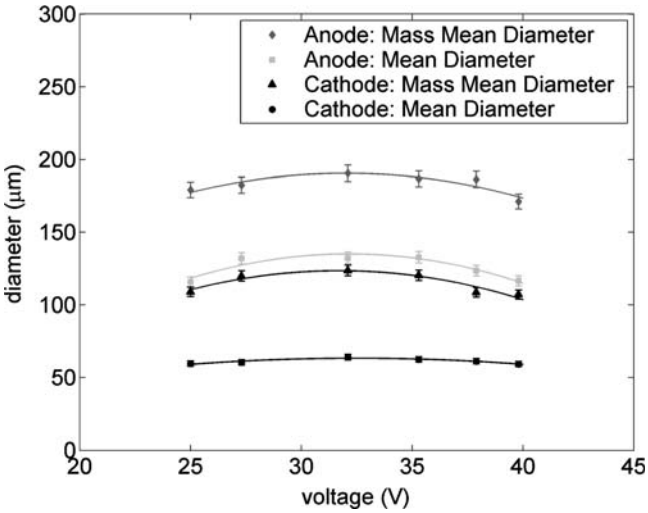

Fig. 11 Mean-diameter and mass-mean-diameter of cathodic and anodic particles as a function of the applied voltage; error-bars represent a standard deviation of 3-5 measurements of about 8000 particles; operating parameters: aluminum wires, p = 515 kPa, wire-feed-rate = 7 m/min, stand-off distance = 50 mm.

tend to produce smaller particles with increasing gas flow velocity (Ref 20).

The primary dimensionless parameter on which secondary atomization depends is the gas Weber number defined as $We = \rho_g \Delta U^2 D/\sigma$, where ρ_g, ΔU, and σ are gas density, relative gas-droplet velocity, and surface tension of the liquid metal. For all metallic melts, there exists a critical Weber number ($We_{crit} \approx 13$) below which droplets remain stable (Ref 20). The Weber number in the nozzle region of the spraying gun, where the primary breakups occur, is estimated to be 70 (assuming typical values for gas velocity and spherical drop diameter as in Ref 10). Thus the metallic detachments are unstable and subject to further disintegration. However, five centimeters downstream from the nozzle exit, the Weber number dramatically drops to an approximate low value of 0.5, below the critical value. Therefore, the effect of secondary disintegrations can be neglected in the spray region. This is confirmed by experimental results that showed no significant change in the size distribution along the spray, discussed in Sec. 3.

Because the size of droplets resulting from a secondary breakup is proportional to the size of the original particle (Ref 20) and because the primary breakups from anode and cathode are different in size (Ref 10), the size of anodic and cathodic droplets after the secondary atomization should be distinct.

Figure 10 shows the variation in particle size with wire feed rate. There was a small increase in particle diameter as feed rate increases, though it was so small it was difficult to see the effect on mass mean diameter. Increasing the wire feed rate shortens the arcing distance, which results in an increase in the current that passes through the arc, and therefore the heat flux to the electrodes. In the case of the cathode, where heating is localized at the cathode spot, the increased heat flux results in faster detachment of the same size droplets from the wire material, which is fed at a higher rate. In the anode region, where heating is is spread over a larger area, the increased heat flux results in a thicker layer of molten material, which is pushed away by the drag force of the gas flow. The drag force, however, does not increase with the thickness of the anode sheets, and therefore slightly larger particles are produced in the anode.

Varying operating voltage, too, had only a small effect on particle size. Figure 11 shows the variation of mean particle diameter with voltage. A midvalue voltage at about 32 V appeared to maximize particle size. A full explanation of this behavior will likely require a detailed analysis of changes in heat transfer and magnetic forces at the wire tip caused by varying voltage.

6. Conclusions

In a wire-arc spray system, particles are formed by atomization of molten metal from the tips of two wires between which an electric arc is struck. The arc attaches to the anode over a much larger area than it does for the cathode, and consequently, particles separating from the anode are larger than those from the cathode. In-flight particles are a mixture of cathodic and anodic particles. The size distributions of the two sets of particles can be identified and separated by assuming that both follow a log-normal distribution. Experiments showed that increasing the pressure of atomizing gas decreased the size of both anodic and cathodic particles, while changing wire feed rate and operating voltage did not change particle size significantly.

Acknowledgments

The authors would like to acknowledge financial support for this research from the Natural Sciences and Engineering Research Council of Canada (NSERC) and Materials and Manufacturing Ontario (MMO).

References

1. A. Pourmousa, A. Abedini, J. Mostaghimi, and S. Chandra, Particle Diagnostics in Wire-Arc Spraying System, *Thermal Spray 2004: Advances in Technology and Application,* ASM International, May 10-12, 2004 (Osaka, Japan), ASM International, 2004, p 962-968.
2. M.P. Planche, H. Liao, and C. Coddet, Relationships between In-flight Particle Characteristics and Coating Microstructure with a Twin Wire Arc Spray Process and Different Working Conditions, *Surf. Coat. Technol.,* Vol 182, 2004, p 215-226
3. G. Jandin H. Liao, Z.Q. Feng, and C. Coddet, Correlations between Operating Conditions, Microstructure and Mechanical Properties of Twin Wire Arc Sprayed Steel Coatings, *Mater. Sci. Eng.,* A349, 2003, p 298-305
4. X. Wang, D. Zhuang, E. Pfender, J. Heberlein, and W. Gerberich, Effect of Atomizing Gas Pressure on Coating Properties in Wire Arc Spray, *Thermal Spray Industrial Applications,* C.C. Berndt and S. Sampath, Ed., June 20-24, 1994 (Boston, MA), ASM International, 1994, p 587-592
5. N.A. Hussary and J. Heberlein, Investigations of Arc Behavior and Particle Formation in the Wire Arc Spray Process Using High Speed Photography, *Thermal Spray: Surface Engineering via Applied Research,* C.C. Berndt, Ed., May 8-11, 2000 (Montréal, Québec, Canada), ASM International, 2000, p 737-742
6. N.A. Hussary and J.V.R. Heberlein, Primary Breakup of Metal in the Wire Arc Spray Process, *Thermal Spray 2003: Advancing the Science and Applying the Technology,* B.R. Marple and C. Moreau, Ed., May 5-8, 2003 (Orlando, FL), ASM International, 2003, p 1023-1032
7. T. Watanabe, X. Wang, E. Pfender, and J. Heberlein, Correlations between Electrode Phenomena and Coating Properties in Wire Arc Spraying, *Thin Solid Films*, Vol 316, 1998, p 169-173
8. T. Watanabe, T. Sato, and A. Nezu, Electrode Phenomena Investigation of Wire Arc Spraying for Preparation of Ti-Al Intermetallic Compounds, *Thin Solid Films,* Vol 407, 2002, p 98-103
9. Y.L. Zhu, H.L. Liao, C. Coddet, and B.S. Xu, Characterization via Image Analysis of Cross-over Trajectories and Inhomogeneity in Twin Wire Arc Spraying, *Surf. Coat. Technol.,* Vol 162, 2003, p 301-308
10. M. Kelkar and J. Heberlein, Wire-Arc Spray Modeling, *Plasma Chem. Plasma Proc.,* Vol 22 (No.1), March 2002, p 1-25
11. M. Kelkar, N. Hussary, J. Schein, and J. Heberlein, Optical Diagnostics and Modeling of Gas and Droplet Flow in Wire Arc Spraying, *Thermal Spray: Meeting the Challenges of the 21st Century,* C. Coddet, Ed., May 25-29, 1998 (Nice, France), ASM International, 1998, p 329-334
12. J.C. Amson, An Analysis of the Gas Shielded Consumable Metal Arc Welding System, *Brit. Weld. J.,* April 1962, p 232-249
13. T. Arai and H. Hashimoto, Disintegration of a Thin Liquid Sheet in a Concurrent Gas Stream, *Proceedings of the 3rd International Conference on Liquid Atomization and Spray Systems,* 1985 (London), The Institute of Energy, London, England, p VIB/1/1-7
14. L. Pouliot, J. Blain, and F. Nadeau, *DPVOS Reference Manual*, Revision 5.0, TECNAR Automation Ltd., St-Hubert, QC, Canada, July 1999
15. R. Bolot, R. Bonnet, G. Jandin, and C. Coddet, Application of CAD to CFD for the Wire Arc Spray Process, *Thermal Spray 2001: New Surfaces for a New Millennium,* C.C. Berndt, K.A. Khor, and E.F. Lugscheider, Ed., May 28-30, 2001 (Singapore), ASM International, 2001, 1381 p 889-894
16. J. Jenista, J. Heberlein, and E. Pfender, Numerical Model of the Anode Region of High-Current Electric Arcs, *IEEE Trans. Plasma Sci.,* Vol 25 (No. 5), 1997, p 883-890
17. G. Saevarsdottir, M.T. Jonsson, and J.A. Bakken, A Novel Approach to Cathode/Anode Modelling for High-Current AC Arcs, Plasma Processes and Polymers: 16th International Symposium on Plasma Chem., R. d'Agostino, P. Favia, F. Fracassi, and F. Palumbo, Ed., 22-27 June 2003 (Taormina, Italy), Tipolito Vitetum, Bitetto, Italy, 2003, p 146
18. A.H. Lefebvre, *Atomizations and Sprays,* Hemisphere Pub. Corp., NY, 1989
19. R. Ghafouri-Azar, J. Mostaghimi, S. Chandra, and M. Charmchi, A Stochastic Model to Simulate the Formation of a Thermal Spray Coating, *J. Therm. Spray Technol.,* Vol 12 (No. 1), 2003, p 53-69
20. A.J. Yule and J.J. Dunkley, *Atomization of Melts for Powder Production and Spray Deposition,* Oxford, University Press, 1994, p 43